Particle and Aerosol Research 제 5 권 제 3 호
PAAR Vol. 5, No. 3 (2009) pp. 111～122
(사)한국입자에어로졸학회

총 설

Synthesis of aerosol nanoparticles by spark discharge and applications

Jaehong Park, Jeong Hoon Byeon, Ki Young Yoon, Jae Hong Park and Jungho Hwang*
Department of Mechanical Engineering, Yonsei University, Seoul, Korea

(Received 1 september 2009, accepted 8 september 2009)

Abstract

This paper reviews about synthesis of nanoparticles by spark discharge and applications. A method of catalytic activation with Pd and Pt aerosol nanoparticles produced by spark discharge was introduced. After annealing, the catalytically activated substrate placed into a solution for electroless silver deposition. The silver was then formed only on the activated regions of the substrate. Silver line patterns having a width of 18 μm and a height of 1 μm were created with the ability to be effectively reproduced. Antimicrobial nanoparticles such as silver were used for removal of bioaerosols. Silver nanoparticles deposited air filters such as ACF filters were evaluated by antimicrobial test.

Key words : Nanoparticles, Spark generation, Electroless deposition, Patterning, Antimicrobial

1. INTRODUCTION

The generation of metallic nanoparticles has mainly been carried out in liquid solutions containing metal ions, reductants, and some polymers (protecting agents) (Devarajan *et al.*, 2005). Recently, considerable attention has been focused on the characteristics of "naked" metal nanoparticles (Harada *et al.*, 2005), which are believed to be appropriate for examining the effect of surface structure and geometry. Methods for generating naked metallic nanoparticles include pyrolysis, chemical vapor deposition, and sputtering. However, these processes demand either high temperatures or a high vacuum environment, which are expensive to operate (Lu and Lin, 2000).

*Corresponding author.
Tel : +82-(0)2-2123-2821, E-mail : hwangjh@yonsei.ac.kr

Spark discharge has been used to generate monometallic particles of a wide range of conducting materials with particles sizes ranging from several nanometers up to ~100 μm in an aerosol state because spark discharge is simple, easily deliverable, and environmental friendly (Schwyn *et al.*, 1988; Watters *et al.*, 1989; Evans *et al.*, 2003; Horvath and Gangl, 2003; Kim and Chang, 2005; Borra, 2006; Simonin *et al.*, 2007). The nanoparticles synthesized from the spark discharger are used as seed catalytic particles for helping deposition of functional materials such as silver. These catalyst nanoparticles are forced to deposit on a target surface (activation process). After the catalytic activation process, functional nanoparticles are deposited by electroless deposition (ELD). The ELD of metal refers to the deposition of a metal onto a substrate, without an external electric current, via oxidation-reduction reactions.

Figure 1 shows the process of nanoparticles genera-

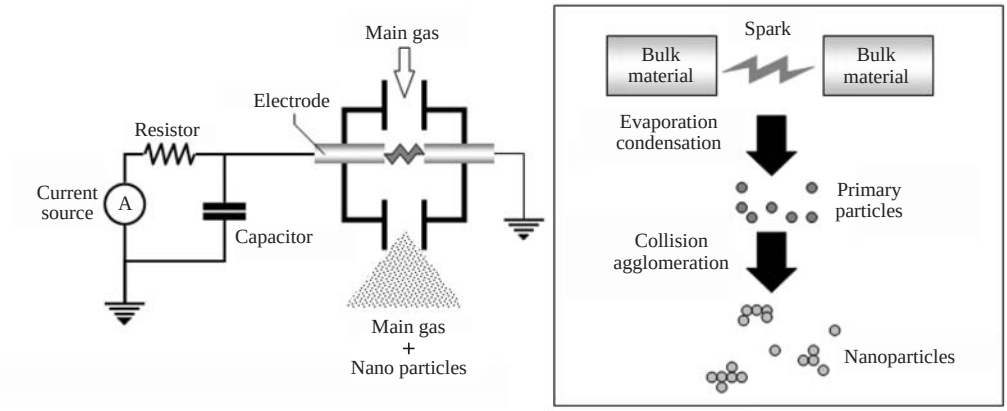

Figure 1. Nanoparticles generation by spark discharger.

tion via spark discharger. When a voltage higher than breakdown voltage is supplied to metal electrodes, it discharges in a spark across the electrode gap, vaporizing material from the electrodes and producing primary particles of a few nm in diameter by nucleation of the vapor. These particles are carried by a flow of main gas and they grow in size due to coagulation or coalescence (Roth *et al.*, 2004; Byeon *et al.*, 2008a).

This paper reviews about synthesis of nanoparticles by spark discharge and applications. Pd, Pt were selected as catalyst nanoparticles used in aerosol activation for different purposes; Pd for catalytic materials, Pt for micro patterning, Pd for antimicrobial. In all these applications, Ag was selected as functional nanoparticle obtained used in ELD, which was performed after the aerosol activation.

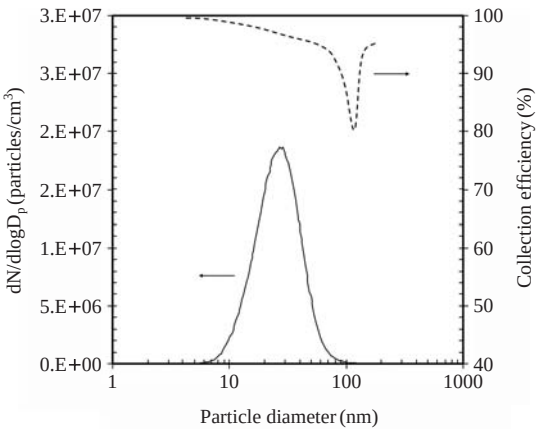

Figure 2. Particle size distribution of spark-generated aerosol nanoparticles and collection efficiency of ACFs.

2. CATALYTIC MATERIAL GENERATION

Porous carbon materials, due to their extensive specific surface area, high adsorption capacity, microstructure, and special surface reactivity, have been widely used in separation, purification, and catalytic processes (Byoen *et al.*, 2007). Activated carbon fibers (ACFs), highly microporous carbon materials, are commercially available in the form of fiber tows, cloths (fabrics), papers, mats, and felts. ACFs have a larger micropore volume and a more uniform micropore size distribution than granular activated carbons (GACs) and, thus, are considered to have a larger adsorption capacity and greater adsorption and desorption rates. The ACFs may be packed or constructed to fit almost any geometry for almost any catalytic application and satisfy the requirements of high catalyst effectiveness and a low pressure drop for finely divided catalysts, but avoid the technical problems associated with powders.

A method of catalytic activation with palladium aerosol nanoparticles produced by spark generation was

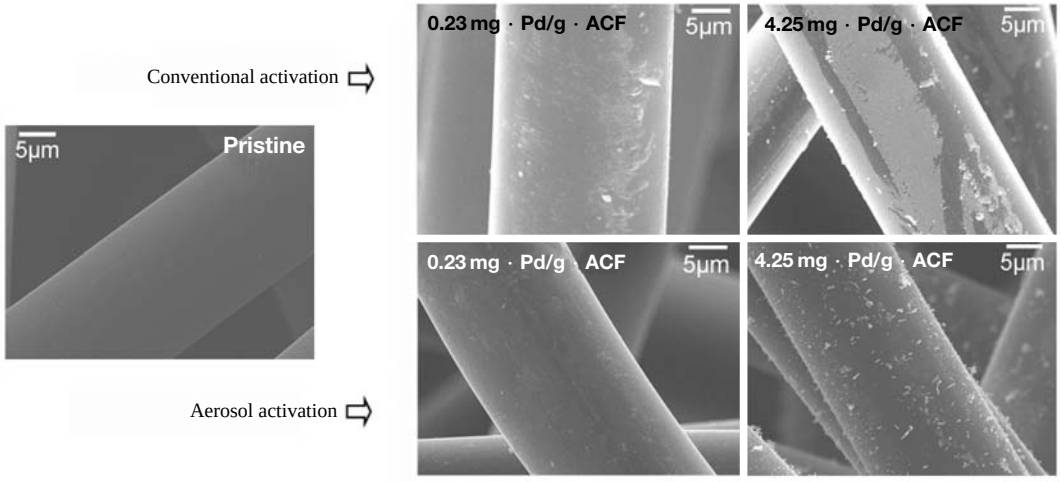

Figure 3. SEM micrographs of conventionally activated and aerosol-activated ACFs.

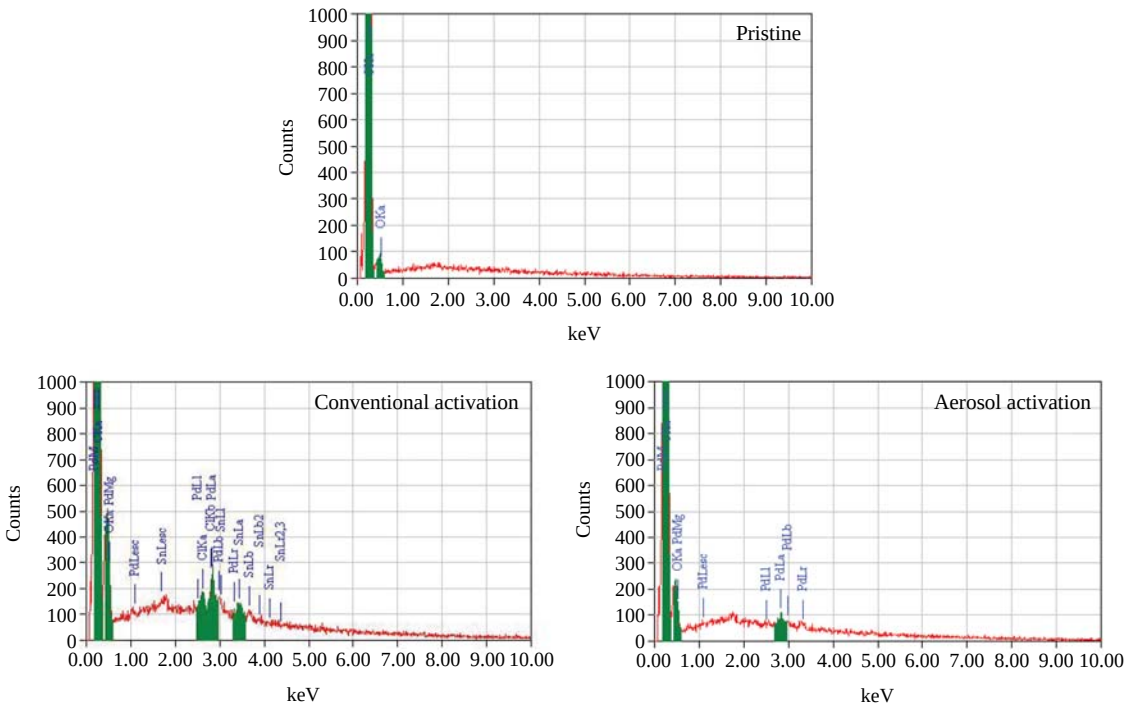

Figure 4. EDX profiles of conventionally activated and aerosol-activated ACFs.

introduced. These catalytic particles were deposited onto the surfaces of ACFs. After thermal curing, the catalytically activated ACFs were placed into a solution for ELD of silver (Byeon *et al.*, 2008b).

Figure 2 shows the size distribution of spark-generated aerosol nanoparticles measured using the scanning

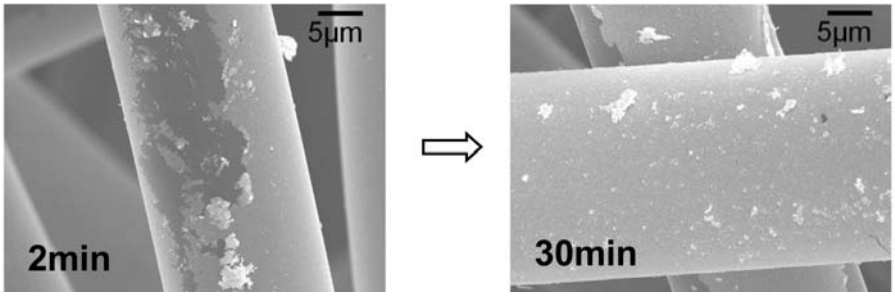

Figure 5. SEM micrographs of particle-deposited ACFs vs ELD time.

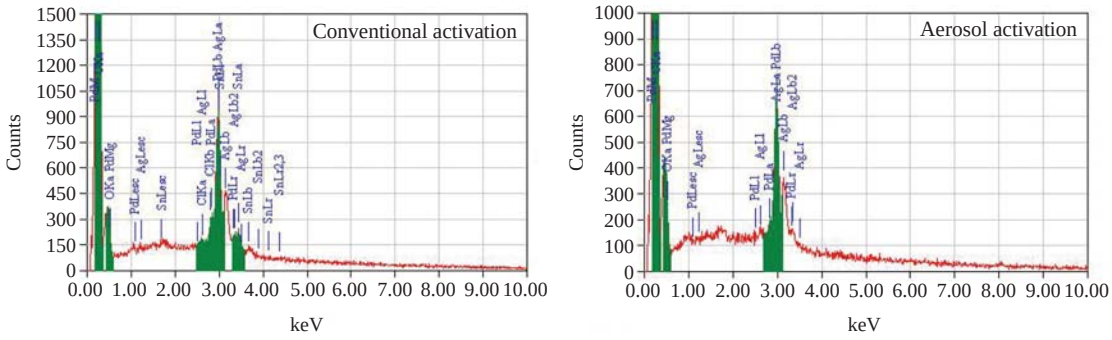

Figure 6. EDX profiles of particle-deposited ACFs (10 min of ELD, 1.42 mg of Pd/g of ACF).

mobility particle sizer (SMPS) system. The geometric mean diameter and geometric standard deviation were 25.5 nm and 1.54, respectively. The total number concentration was 8.8×10^6 particles/cm^3. Figure 2 also shows the fractional (grade) collection efficiency of ACFs as a function of particle size. The efficiency is defined by

$$\eta_{ACF}(d_p) = 1 - [C_{ACF}(d_p)/C_0(d_p)] \quad (1)$$

where $C_0(d_p)$ is the free-stream concentration of the particles and $C_{ACF}(d_p)$ is the concentration after filtration by the ACFs. The morphology and structure of the nanoparticles were characterized by high-resolution transmission electron microscope (HRTEM) and x-ray photoelectron spectroscopy (XPS), respectively.

Figure 3 shows SEM micrographs of conventionally activated (wet chemical process) and aerosol-activated ACFs. While pristine ACFs had a clean surface, in any activation, more particles were deposited on the ACFs by increasing the activation intensity from 0.23 to 4.25 mg of Pd/g of ACFs. From the energy dispersive x-ray (EDX) analyses (Figure 4), it was found that the pristine sample contained carbon and oxygen, which may have originated from the ACFs, while any activated sample contained a small amount of Pd. The conventionally activated sample also contained a small amount of tin and chlorine, which may have originated from tin sensitization and Pd activation.

Figure 5 shows the trend of particle deposition on aerosol activated ACFs with ELD time at an activation intensity of 1.42 mg of Pd/g of ACFs. From the EDX analyses (Figure 6), it was found that the coated metal was mainly comprised of silver; however, it contained a small amount of Pd. Carbon and oxygen, which may have originated from the ACFs, were also detected. For the conventionally activated ACF, tin and chlorine were

Table 1. Textural properties of silver-deposited ACFs vs activation intensity and ELD time.

ELD time (min)	TSSA[a]/MSSA[b]/TPV[c]/MPV[d]/APD[e] (1610/1593/0.87/0.85/17.7 for pristine)			
	0.23 mg of Pd/g of ACFs		4.25 mg of Pd/g of ACFs	
	CA	AA	CA	AA
2	1399/1226/0.72/0.70/17.0	1532/1488/0.80/0.78/17.5	1277/1202/0.65/0.64/16.8	1359/1325/0.72/0.70/17.1
10	1242/1206/0.69/0.67/16.5	1382/1358/0.77/0.76/17.2	1104/1072/0.60/0.57/16.3	1286/1225/0.67/0.65/16.9
30	1091/1003/0.65/0.62/15.9	1284/1236/0.69/0.67/16.6	912/803/0.52/0.51/15.4	1201/1056/0.61/0.59/16.1

[a]Total specific surface aera (m^2/g), [b]Micropore specific surface area (m^2/g), [c]Total pore volume (cm^3/g), [d]micropore volume (cm^3/g), [e]Average pore diameter (Å)

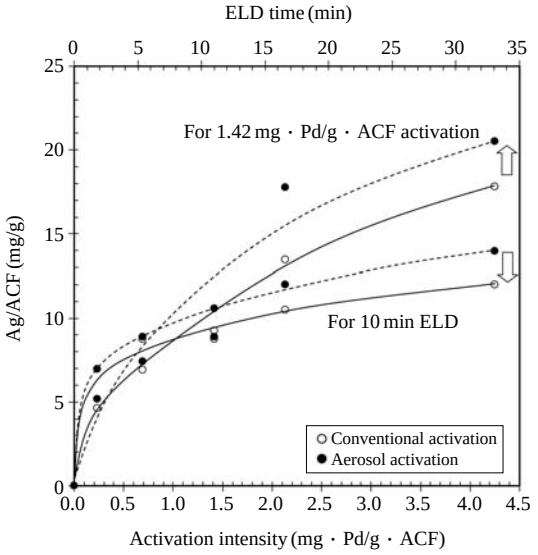

Figure 7. Results of ICP-AES analyses of silver-deposited ACFs.

detected in addition to silver, Pd, carbon, and oxygen. Figure 7 summarizes the plots of the mass of silver deposited onto the ACFs as a function of the activation intensity (for an ELD time of 10 min) and ELD time (at an activation intensity of 1.42 mg of Pd/g of ACFs).

Detailed results of the textural properties of the samples are summarized in Table 1. When either the activation intensity or ELD time was increased in our aerosol activation, the decrease in the specific surface areas, pore volumes, and average pore diameters was less than that in the conventional activation.

Using our aerosol activation and ELD, it was possible to create stable metal layers on ACFs. When the activation intensity increased from 0.23 to 4.25 mg/g (palladium/ACFs) for an ELD time of 10 min, our aerosol activation increased the silver deposition from 7.1 to 13.2 mg/g (silver/ACFs) and the average size of the silver particles from 4.9 to 38.8 nm. However, the surface area and pore volume of the ACFs decreased from 1382 to 1286 m^2/g and from 0.77 to 0.67 cm^3/g, respectively. Our aerosol activation method can be applied to activate porous carbon objects of different thicknesses with the appropriate selection of flow direction, flow velocity, and number of sparks generated.

3. MICRO PATTERNING

There is great interest in the fabrication of micro- and nanopatterned metallic structures on substrates for a wide range of electronic, photonic, and magnetic devices, including semiconductor logic and memory devices, photovoltaic cells, displays, and magnetic storage (Hagberg *et al.*, 2007). The ELD of metal is a convenient, inexpensive metallization technique that works on nano- or microsized objects and can be used to pattern 2D and 3D structures (Charbonnier *et al.*, 2004; Yangimoto *et al.*, 2005). Since ELD requires surface activation with a metal catalyst, such as palladium and platinum, many researchers have investigated ways to advance the activation by combining photochemical (Hozumi *et al.*, 2005), chemical (Khoperia *et al.*, 1997), imprinting (Hagberg *et al.*, 2007), and self-assembled block copolymer tools in order to grow site-selective catalyst.

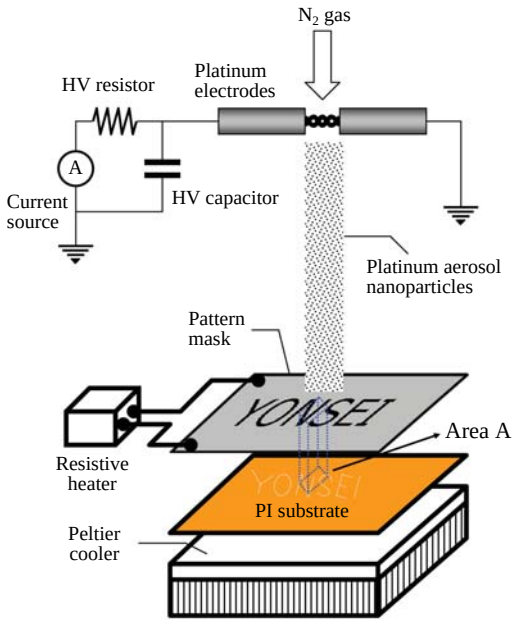

Figure 8. Site-selective catalytic surface activation via aerosol nanoparticles for use in metal micro patterning.

Our technique does not need any special devices such as laser, UV, plasma, and electron beams nor does it require special preparations such as catalyst colloid solutions. We enhanced the deposition of platinum aerosol particles onto a flexible polyimide (PI) substrate by controlling the thermophoresis, which is a physical phenomenon in which aerosol particles, subjected to a temperature gradient, move from high- to low-temperature zones of the gas. Without any chemical pretreatment, we were able to reproduce a stable and selective deposition of particles on the PI substrate through a pattern hole. After annealing, the catalytically activated PI substrate was immersed in a silver ELD solution that resulted in the ELD of silver on the platinum nanoparticles of the PI substrate.

Figure 8 shows an overview of site selective catalytic surface activation. The platinum nanoparticles were generated via spark discharge and carried by N_2 gas to a PI substrate through the pattern hole (width, 100 μm; depth, 100 μm) of the "YONSEI" mask (Debora Electronics Co., Ltd., Korea) for a duration of 5 min (Byeon *et al.*, 2008c).

The size distribution of the platinum nanoparticles was measured using a SMPS and is provided in Figure 9a. The electrical mobility diameter of the particles ranged from 20 to 200 nm. The morphology and structure of the particles were characterized by a HRTEM selected area electron diffraction (SAED) pattern and XPS. For the characterizations, the airborne particles were directly sampled on a porous carbon-coated copper grid. The HRTEM micrograph (inset of Figure 9a) reveals that the platinum particles were agglomerates of several primary particles (each ~26Å in diameter). Figure 9b shows the SAED pattern corresponding to the HRTEM micrograph. Figure 9c shows the XPS profile for the particles revealing that the particles were pure platinum. The binding energy (BE) doublet with the BEs for the Pt $4f_{7/2}$ and Pt $4f_{5/2}$ peak components lying at about 71.1 and 74.4 eV, respectively, are assigned to the Pt^0 species. Figure 9d shows a FESEM image of the particles in a line of the pattern. The FESEM image shows that the particles are spread out over the entire line. The FESEM image also shows that the thermophoretic focusing of the particles resulted in a line width of ~8 μm, which is much narrower than the width of the hole (100 μm) in the mask.

Figure 10a shows a photo of the silver pattern. The optical microscopy analysis of Figure 10a revealed that line patterns having a width of 18 μm were obtained (Figure 10b). As shown in Figure 10b, the silver ELD occurred only on the platinum nanoparticles, i.e., at the activated region of the PI substrate. The platinum nanoparticles effectively acted as a seed to initiate the silver ELD. The line width of silver patterns (18 μm) was wider than that of platinum patterns (~8 μm, as shown in Figure 9d) because ELD is an isotropic process. A FESEM picture of a silver line pattern shows that silver particles were densely packed (Figure 10c). From the EDX analysis (Figure 10d) it was found that the coated metal consisted mainly of silver but contained a small amount of platinum as well as carbon and oxygen, which may have originated from the PI substrate. The XRD profile of the silver pattern shows that there exist

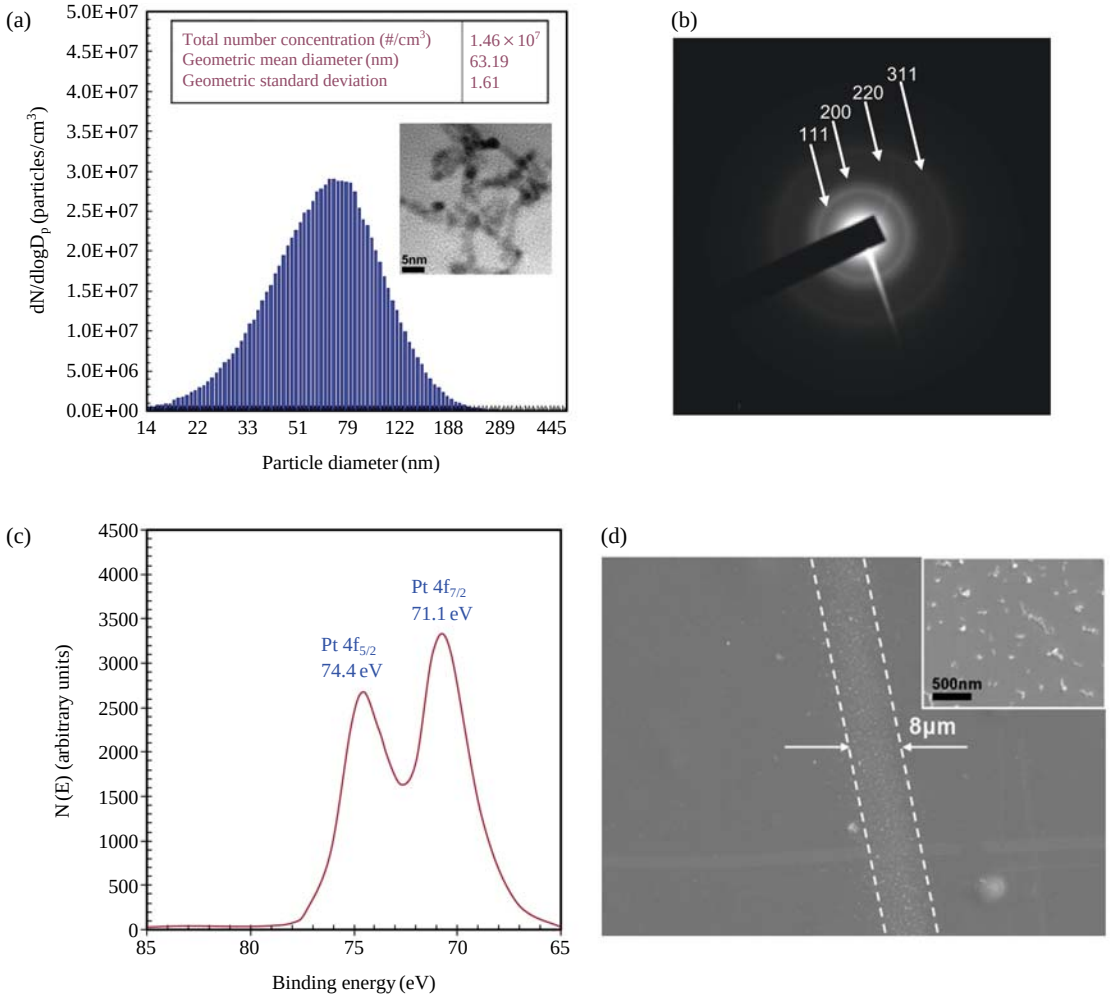

Figure 9. Particle characterization of aerosol activation. (a) Particle size distribution with a HRTEM image (inset) of spark-generated platinum particles. (b) SAED pattern of the particles. (c) XPS profile of the particles. (d) FESEM image of the pattern in the PI substrate.

five peaks located at 2θ=38.2°, 44.4°, 64.5°, 77.5°, and 81.6° (Figure 10e). Compared with the data from the powder diffraction file No. 04-0783, these peaks correspond to the [111], [200], [220], [311], and [222] planes of the fcc phase for silver. The XRD profile shows the characteristics of pure metallic silver with a good crystallinity and without any impurity phase. The average particle size evaluated according to Scherrer's formula was approximately 35 nm.

Resistivities (ρ) of the silver pattern were calculated through the relationship $\rho = RA/L$, where R, A, and L are the resistance, cross-sectional area, and length of the pattern, respectively. The average value of the resistivities was approximately 6.8 μΩ · cm, which is almost comparable to the theoretical resistivity of bulk silver (1.6 μΩ · cm).

Figure 11 shows silver micropatterns containing square dot array, line, line array, Y-branched line, and tapered line using different pattern masks were also demonstrated.

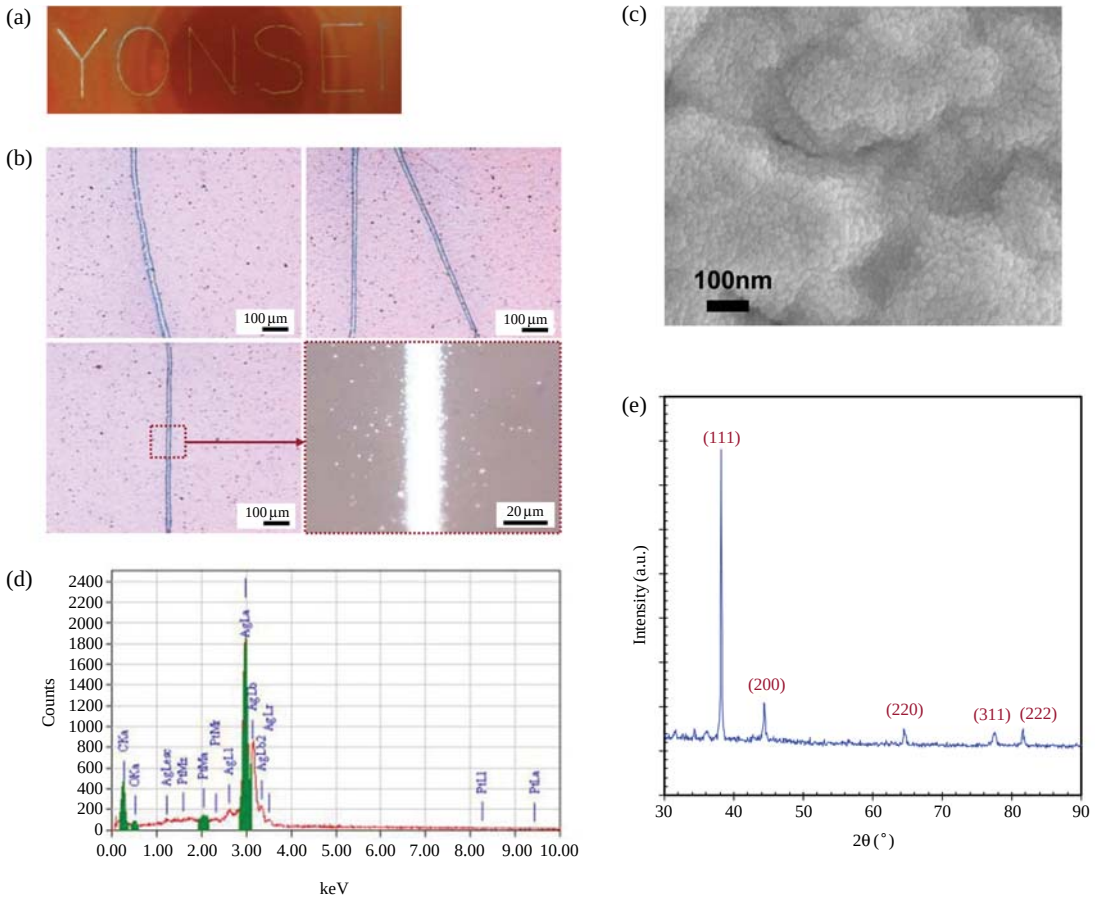

Figure 10. Results of silver ELD. (a) Photo of the silver pattern. (b) Optical microscopy images of the silver pattern. (c) FESEM micrograph corresponding to the optical microscopy images. (d) EDX profile. (e) XRD profile.

Using site-selective aerosol activation and ELD processes it was possible to create stable and selective silver patterns with micrometer dimensions on a flexible PI substrate. Our processes were simple and environmentally benign and can be applied in order to produce display electronics circuits, sensors, radiofrequency identification (RFID) transponders, and other microelectronic devices.

4. ANTIMICROBIAL TEST WITH METALLIC NANO PARTICLES

Bioaerosols are airborne particles of biological origins, including viruses, bacteria, fungi, and all varieties of living materials. They are known as etiological agents of many diseases such as anthrax, SARS (severe acute respiratory syndrome), asthma, and so on. Bioaerosols of indoor air accumulate on the filters of heating, ventilating and air conditioning (HVAC) systems in large quantities, and are able to multiply there under certain conditions, especially if high amounts of moisture on the filter are present (Schleibinger and Rüden, 1999). Table 2 shows various kinds of microorganisms from indoor air (Yoon *et al.*, 2008).

Antimicrobial treatment is required on air filters such as ACF filter. Well-known antimicrobial materials such as silver react with proteins by combining the -SH

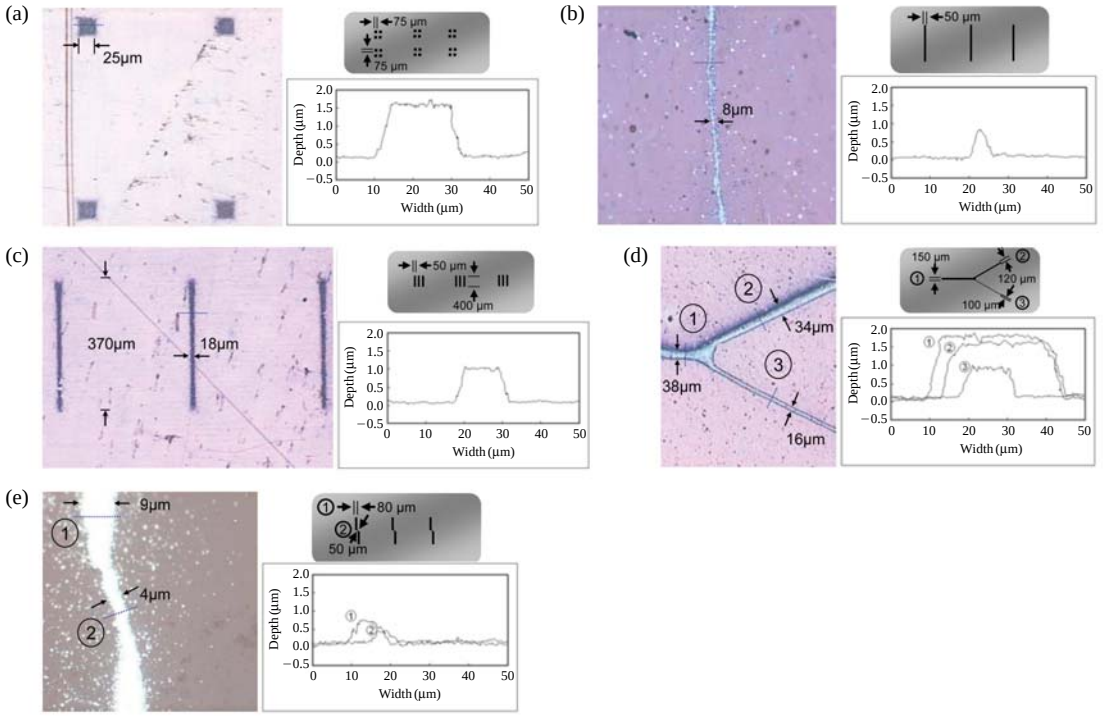

Figure 11. Optical microscope image, schematics of pattern mask, and cross-sectional profile for other silver micropatterns: (a) square dot array, (b) line, (c) line array, (d) Y-branched line, and (e) tapered line.

Table 2. Microorganisms identified from indoor air.

Microorganisms (Analytical method)	Species identified
Bacteria (API Kit)	*Corynebacterium striatum*, *Staphylococcus lugdunensis*, *Staphylococcus epidermidis*, *Sphingomonas paucimobilis*, *Bacillus mycoides*, *Bacillus pumilus*, *Rhodococcus* spp., *Micrococcus* spp.
Fungi (GC)	*Aspergillus niger*, *Aspergillus fumigatus*, *Acremonium* spp., *Exophiala jeanselmei*, *Penicillium* spp.
Actinomycetes (GC)	*Nocardiopsis dassonvillei*, *Streptomyces lavendulae*, *Streptomyces halstedii*

Table 3. Diameters of the inhibition zones of the silver deposite ACF filters (mm).

Activation type	Raw ACF	Aerosol activation				Conventional activation			
Activation intensity (mg)	0	0.12	0.36	0.73	2.19	0.12	0.36	0.73	2.19
S. epidermidis	10	11	12	12	13	12	12	12	13
E. coli	10	12	12	12	12	12	12	12	12

groups of enzymes; consequently, this reaction leads to the inactivation of the proteins (Jeon *et al.*, 2003).

We enhanced the deposition of Pd aerosol particles onto an ACF filter. After annealing, the catalytically activated ACF filter was immersed in a silver ELD solution that resulted in the ELD of silver on the Pd nanoparticles of the ACF filter.

The antimicrobial effects of the silver-deposited ACF

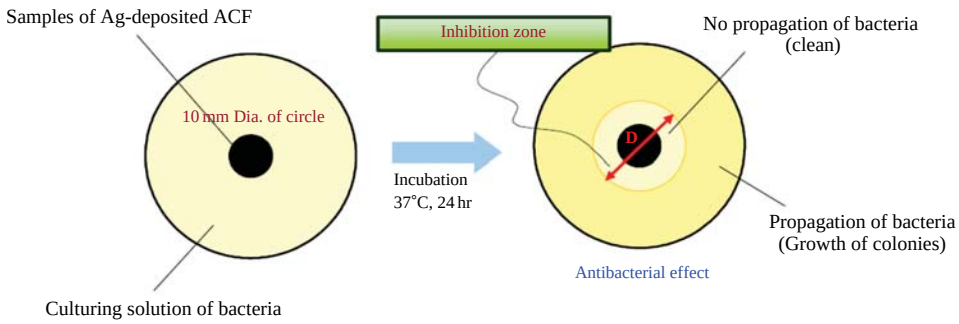

Figure 12. Schematic of disk-diffusion method.

(a) *S. epidermidis* (Gram positive)

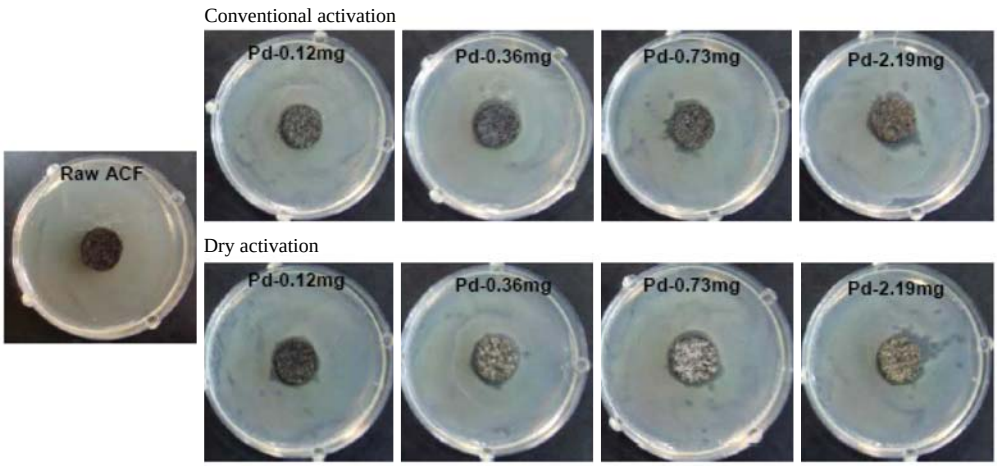

(b) *E. coli* (Gram negative)

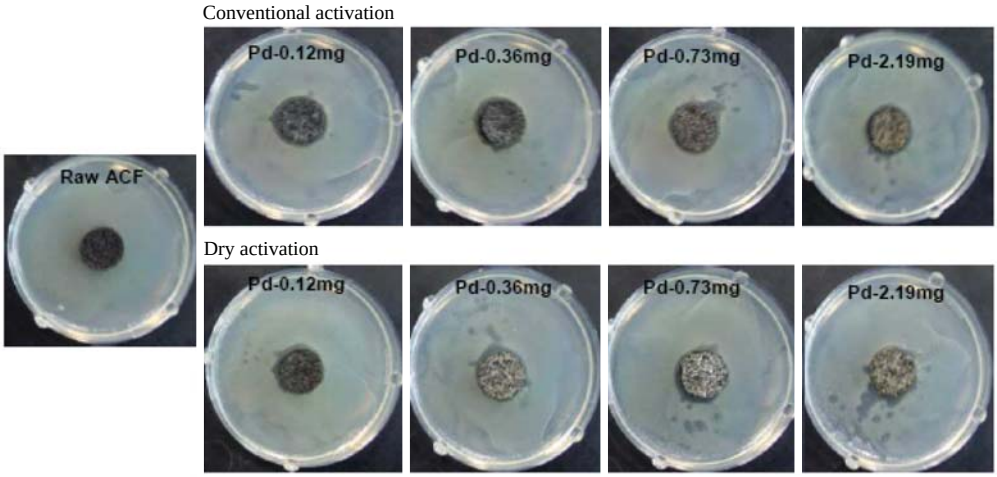

Figure 13. Results of disk-diffusion method of silver nanoparticles deposited ACF filter.

filters were also characterized using the disk-diffusion method (Figure 12) and the results are represented by inhibition zone diameters in Table 3. Nutrient agar, made by dissolution of 5 g of peptone, 3 g of meat extract, and 15 g of bacto agar in 1,000 mL of deionized water, was used to culture the bacteria after autoclave. 0.1 mL of the prepared bacterial suspension for *E. coli* or *S. epidermidis* was spread on the nutrient agar plate. The test filter was placed on the lawn of bacteria and incubated overnight. Figure 13 shows silver nanoparticles deposited ACF filter when the Pd activation intensity increased from 0.12 to 2.19 mg for an ELD time of 10 min. The antimicrobial activity was observed by visually inspecting the diameter of the inhibition zone around the filter. For the silver deposited ACF filters, the bacteria did not grow within or around the filters, while the bacteria did grow on the pristine ACF filter (Ko, 2006).

5. CONCLUSIONS

Using our aerosol activation and ELD, it was possible to create stable metal layers on ACFs, When the activation intensity increased from 0.23 to 4.25 mg/g (palladium/ACFs) for an ELD time of 10 min, our aerosol activation increased the silver deposition from 7.1 to 13.2 mg/g (silver/ACFs) and the average size of the silver particles from 4.9 to 38.8 nm.

With patterning test, thermophoretically depositing the Pt particles onto a flexible PI substrate through the pattern hole of a mask was realized. After annealing, the catalytically activated substrate was placed into a solution for silver ELD. The silver was then formed only on the activated regions of the substrate. Silver line patterns having a width of 18 μm and a height of 1 μm are created with the ability to be effectively reproduced. The average value of the resistivities was approximately 6.8 μΩ · cm, which is almost comparable to the theoretical resistivity of bulk silver (1.6 μΩ · cm).

Silver nanoparticles were selectively deposited ACF filter when the Pd activation intensity increased from 0.12 to 2.19 mg for an ELD time of 10 min. The antimicrobial activity was observed by visually inspecting the diameter of the inhibition zone around the filter. For the silver deposited ACF filters, the bacteria did not grow within or around the filters, while the bacteria did grow on the pristine ACF filter

ACKNOWLEDGEMENT

This work was supported by the National Research Foundation (NRF) grant funded by the Korea government (MEST) (No. 20090073212).

REFERENCES

Borra, J.P. (2006). Nucleation and aerosol processing in atmospheric pressure electrical discharges: Powders production, coatings and filtration. *Journal of Physics D*, 39, 19-54.

Byeon, J.H., Park, J.H., and Hwang, J. (2008a). Spark generation of monometallic and bimetallic aerosol nanoparticles, *Journal of Aerosol Science*, 39, 888-896

Byeon, J.H., Ko, B.J., and Hwang, J. (2008b). Catalytic activaton of activated carbon fibers cia palladium aerosol nanoparticles for use in electroless silver deposition, *Journal of Physical Chemistry C*, 112, 3627-3632.

Byeon, J.H., Park, J.H., Yoon, K.Y., and Hwang, J. (2008c). Site-selective catalytic surface actication via aerosol nanoparticles for use in metal micropatterning, *Langmuir*, 24, 5949-5954.

Charbonnier, M., Goepfert, Y., Romand, M., and Leonard, D. (2004). Electroless plating of glass and silicon substrates through surface pretreatment involving plasma-polymerization and grafting processes, *Adhes*, 80, 1103-1130.

Devarajan, S., Bera, P., and Sampath, S. (2005). Bimetallic nanoparticles: Asingle step synthesis, stabilization, and characterization of Au-Ag, Au-Pd, and Au-Pt in sol-gel derived silicates, *Journal of Colloid and Interface Science*, 29, 117-129.

Evans, D.E., Harrison, R.M., and Ayres, J.G. (2003). The generation and characterization of elemental carbon aerosols for human challenge studies, *Journal of Aerosol Science*, 34, 1023-1041.

Hagberg, E.C., Scott, J.C., Shaw, J.A., von Werne, T.A., Mae-

gerlein, J.A., and Carter, K.R. (2007). Mold and metallization: nanocontact molding for the fabrication of metal structures, *Small*, 3, 1703-1706.

Harada, M., Toshima, N., Yoshida, K., and Isoda, S. (2005). Aggregated structure analysis of polymer-protected platinum/Ruthenium colloidal dispersions using EXAFS, HRTEM, and electron diffraction measurements, *Journal of Colloid and Interface Science*, 283, 64-78.

Horvath, H., and Gangl, M. (2003). A low-voltage spark generator for production of carbon particles, *Journal of Aerosol Science*, 34, 1581-1588.

Hozumi, A., Asakura, S., Futa, A., and Shirahata, N. (2005). Site-selective electroless plating on amino-terminated diamond substrate patterned by 126 nm vacuum ultraviolet light lithography, *Journal of Vacuum Science and Technology A*, 23, 1029-1033.

Jeon, H.J., Yi, S.C., and Oh, S.G. (2003). Preparation and antibacterial effects of Ag-SiO_2 thin films by sol-gel method, *Biomaterials*, 24, 4921-4928.

Khoperial, T.N., Tabatadze, T.J., and Zedgenidze, T.I. (1997). Formation of microcircuits in microelectronics by electroless deposition, *Electrochimica Acta*, 42, 3049-3055.

Kim, J.T., and Chang, J.S. (2005). Generation of metal oxide aerosol particles by a pulsed spark discharge technique, *Journal of Electrostatics*, 63, 911-916.

Ko, B.J. (2006). Characterizations of electroless silver deposition on activated carbon fibers by a dry catalytic activation, Master Thesis, Yonsei University Dept. of Mech. Eng., Seoul, Korea, pp. 38-42.

Lu, S.Y., and Lin, Y.Z. (2004). Pd-Ag alloy films prepared by metallorganic chemical vapor deposition process, *Thin Solid Films*, 376, 67-72.

Roth, C., Ferron, G.A., Karg, E., Lentner, B., Schumann, G, Takenaka, S., and Heyder, J. (2004). Generation of ultrafine particles by spark discharging, *Aerosol Science and Technology*, 38, 228-235.

Schleibinger, H., and Rüden, H. (1999). Air filters from HVAC systems as possible source of volatile organic compounds (VOC)-laboratory and field assays, *Atmospheric Environment*, 33, 4571-4577.

Schwyn, S., Garwin, E., and Schmidt-Ott, A. (1988). Aerosol generation by spark discharge, *Journal of Aerosol Science*, 19, 639-642.

Simonin, L., Lafont, U., Tabrizi, U., Schmidt-Ott, A., and Kelder, E.M. (2007). Sb/O nano-composites produced via spark discharge generation for Li-ion battery anodes, *Journal of Power Sources*, 174, 805-809.

Watters, Jr., R.L., DeVoe, J.R., Shen, F.H., Small, J.A., and Marinenko, R.B. (1989). Characteristics of aerosols produced by the spark discharge, *Analytical Chemistry*, 61, 1826-1833.

Yanagimoto, H., Akamatsu, K., Deki, S., and Gotoh, K. (2002). Novel copper electroless plating process on ceramic substrate using copper oxide particle, *Solid State Latter*, 5, C87-C89.

Yoon, K.Y., Byeon, J.H., Park, J.H., and Hwang, J. (2007). Susceptibility constant of E.coli and B.subtilis to silver and copper nanoparticles, *Science of the Total Environment*, 373, 572-575.

Yoon, K.Y., Byeon, J.H., Park, C.W., and Hwang, J. (2008). Antimicrobial effect of silver particles on bacterial contamination of activated carbon fibers, *Environmental Science & Technology*, 42, 1251-1255.